UDC 553.43:550.83:004.8
IRSTI 38.35.19

https://doi.org/10.55452/1998-6688-2026-23-2-435-450

[1]*Saduov A.,
Senior Lecturer, ORCID ID: 0000-0003-1501-7772,
*e-mail: a.saduov@satbayev.university
[1]Satbayev University, Almaty, Kazakhstan

UNSUPERVISED DELINEATION OF PROSPECTIVITY ZONES FOR STRATIFORM CU-CO IN THE SOUTHERN COPPERBELT MARGIN (ZAMBIA)

Abstract

This study presents an unsupervised workflow for delineating prospectivity zones for stratiform copper-cobalt mineralization in the southern margin of the Central African Copperbelt, Zambia, using only airborne geophysical data (gravity, magnetics, radiometry, terrain). Three clustering algorithms-K-Means, Fuzzy C-Means (FCM), and Self-Organizing Maps (SOM)-were applied, followed by consensus clustering to isolate robust target zones. Key geophysical filters (tilt derivative, total horizontal derivative, analytic signal) and radiometric ratios (U/Th, U/K) were computed and compared across clusters. The most prospective cluster was validated against literature-calibrated geophysical thresholds and was found to match known exploration criteria and regional structural trends. A final probabilistic prospectivity map was generated from FCM membership, classifying targets into three confidence levels. While lack of drill-hole data prevents quantitative accuracy assessment, this approach demonstrates that fully unlabeled machine learning on airborne data can effectively guide early-stage exploration in data-sparse regions. The proposed workflow offers a reproducible framework for AI-driven prospectivity mapping in frontier terrains.

Keywords: copper-cobalt, unsupervised learning, clustering, airborne geophysics, Zambia.

Received March 2, 2026; accepted May 28, 2026.

Introduction

The Central African Copperbelt (Zambia and the Democratic Republic of the Congo) has been recognized as the world's largest sediment-hosted copper province and a major cobalt source. The Neoproterozoic Katangan basin has been reported to contain ~8.7 billion tonnes of copper ore at ~2.6 wt% Cu, and mineralization along the southern Zambian margin has been interpreted to extend beneath sedimentary cover into greenschist- to amphibolite-facies rocks affected by the Lufilian orogeny [1]. In contrast to the well-drilled northern districts, the Southern Copperbelt Margin has remained weakly constrained by geochemical sampling and drilling, and stratiform Cu–Co potential has therefore been expected to be largely concealed beneath cover [1].

Traditional mineral prospectivity mapping (MPM) approaches, including knowledge-driven overlays and supervised machine-learning models, have been shown to depend on reliable positive (deposit) and negative (barren) labels [2, 3]. In greenfield settings, occurrences are commonly absent and true negatives cannot be verified, which limits the applicability of supervised calibration and can render weakly supervised strategies inconclusive [3]. Consequently, fully unsupervised approaches have been required to delineate exploration targets without deposit labels.

Unsupervised learning has been increasingly used to detect multivariate domains and anomalies directly from geodata. Clustering methods have been applied to delineate coherent geoscientific signature zones, yet many studies have relied on a single algorithm and/or on expert-guided cluster selection. To reduce algorithm-specific bias, a consensus framework has been adopted by integrating

K-Means, Fuzzy C-Means (FCM), and Self-Organizing Maps (SOM), and only areas consistently identified across methods have been retained as high-priority zones [4]. The complementary behaviour of hard partitions (K-Means), gradual memberships (FCM), and topology-preserving mapping (SOM) has been leveraged to improve robustness under label-scarce conditions [5].

Because drill-hole and systematic geochemical data were unavailable, prospectivity was inferred solely from airborne geophysical proxy variables. Magnetic derivatives, including tilt derivative and total horizontal derivative, were used to emphasize structural edges and shallow sources, while analytic signal amplitude was used to highlight source-centred responses. Radiometric ratios (U/Th and U/K) were further used as proxies for alteration and redox-related processes, and the applicability of radiometric criteria in exploration has been supported by regional case studies [6]. These six co-registered layers were used as the core input to the clustering ensemble.

Cluster prioritization was performed by comparing cluster summary statistics to literature-derived thresholds representing geophysical responses expected in favourable structural and alteration settings. This external benchmarking was intended to constrain cluster selection objectively and reduce interpretive subjectivity in the absence of local training data. The study was therefore designed to deliver an objective, data-driven prospectivity map for stratiform Cu–Co mineralization in a true greenfield setting and to demonstrate the utility of ensemble unsupervised analytics for frontier exploration targeting.

Geological and Geophysical Context

Geological Setting

The study area has been located near Chililabombwe and Chingola (northern Zambia) along the southern margin of the Central African Copperbelt. The regional basement has been overlain by the Neoproterozoic Katanga Supergroup (~880-520 Ma), which hosts stratiform Cu-Co mineralization predominantly within the Lower Roan Subgroup. In particular, the carbonaceous Ore Shale Formation at the transition from red-bed siliciclastics to overlying reduced sediments has been reported to contain disseminated chalcopyrite, bornite, and chalcocite hosted by bedding-parallel fabrics and carbonate bands [7].

Late Neoproterozoic to Early Paleozoic Pan-African deformation has been expressed by the Lufilian Arc, a NW-SE-trending fold-and-thrust belt, where northeast-vergent thrusting has emplaced Roan sequences onto pre-Katangan crystalline basement. Basement highs, composed mainly of Paleoproterozoic to Mesoproterozoic granites and gneisses, have been interpreted to control sub-basin segmentation during deposition and to influence the preservation and localization of Cu-Co mineralization; for example, basement ridges have been associated with Roan thinning/absence and ore concentration along ridge flanks.

Along the southern Copperbelt margin, Roan stratigraphy has been largely concealed beneath thrust sheets and younger Kundelungu cover. The Chililabombwe-Chingola district has exemplified this configuration, where high-grade Ore Shale orebodies have been exploited at major operations (e.g., Konkola and Nchanga) and have been interpreted to continue downdip beneath thrusts to depths exceeding 1 km, remaining partly blind at surface. Structural duplication and folding of the Ore Shale horizon have been expected to generate synclines and faulted blocks capable of hosting concealed repeats or extensions of mineralization [7].

Airborne survey and preprocessing

A high-resolution airborne survey (KoBold Metals NRG2155) has been acquired over the study area (2022) and the publicly released dataset has been accessed via Kaggle [8]. Gravity, magnetics, radiometrics, and terrain data have been collected along NE-SW flight lines spaced 200 m apart with orthogonal tie-lines at ~2 km, at a nominal terrain clearance of ~80 m. Instrumentation has been reported to include a cesium-vapor magnetometer, an airborne gravimeter stabilized by GPS/inertial measurements, and a 32 L NaI gamma-ray spectrometer; dual-frequency GPS positioning has been used for georeferencing.

Figure 1 – Geographical location of the airborne survey polygon (red outline) near Chililabombwe-Chingola on the southern margin of the Central African Copperbelt The polygon from the provided KML overlay is draped on Google Earth imagery, showing the proximity to the DRC-Zambia border and known mining areas (yellow outline)

Figure 2 – Simplified geological map of the southern margin of the Central African Copperbelt in northern Zambia (adapted from Porter GeoConsultancy 2024). The Roan Group (hosting stratiform Cu-Co ore) is exposed in the cores of Lufilian fold structures and otherwise concealed beneath Nguba and Kundelungu Group formations. Purple stars indicate major Cu-Co deposits (e.g., Konkola, Nchanga). The survey area (yellow outline) spans a zone of complex thrusting and folding where Roan units are largely hidden, highlighting the potential for concealed mineralization.

Standard corrections and derivative transformations have been applied to prepare analysis-ready layers. Gravity observations have been corrected for latitude, free-air, terrain ($\rho = 2.67$ g cm^{-3}), and Bouguer effects to derive Bouguer anomalies and gravity disturbance grids, followed by computation of first vertical derivative and total horizontal derivative to enhance shallow and lateral density contrasts [10]. Magnetic total-field data have been leveled, diurnally corrected, and reduced to the pole to center anomalies over their sources, and derivative products (first vertical derivative and total horizontal derivative) have been generated for edge enhancement [11]. Tilt derivative and analytic signal amplitude have been computed to emphasize subtle sources and source-centered responses, respectively. Radiometric K, eTh, and eU channels have been noise-filtered using NASVD, and ratio maps (U/Th and U/K) have been produced as proxies for alteration and redox-related processes. A digital terrain model has been derived to provide elevation context.

All layers listed in Table 1 have been resampled to a common 50 m grid (WGS84 UTM Zone 35S).

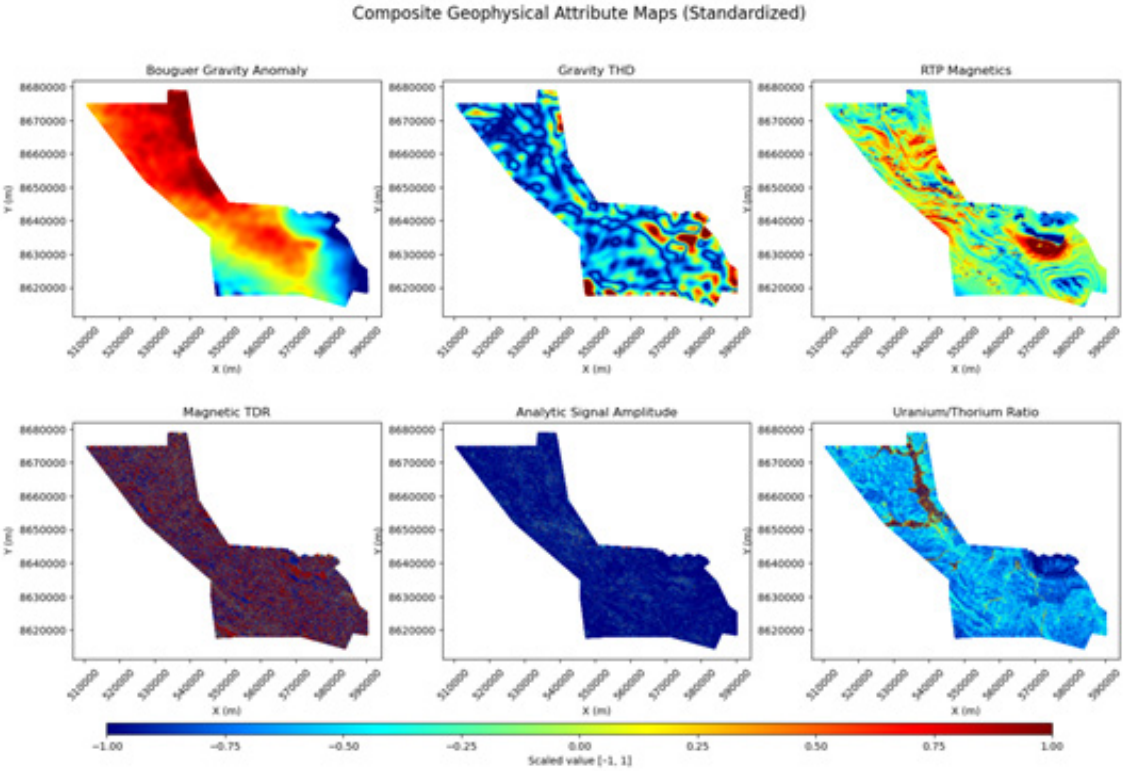

Figure 3 – Composite geophysical attribute maps (standardized) for the airborne survey area. Top row (left to right): Bouguer gravity anomaly; gravity total horizontal derivative (THD); reduced-to-pole (RTP) magnetic intensity. Bottom row (left to right): magnetic tilt derivative (TDR); analytic signal amplitude; uranium/thorium (U/Th) ratio

Table 1 – Summary of input geophysical and radiometric data layers from the airborne survey (NRG2155). All grids are 50 m resolution

Data Layer	Description (Measurement)
X, Y	Coordinates (projection: WGS84 UTM Zone 35S, in meters)
Bouguer267_Processed	Bouguer gravity anomaly (terrain-corrected, density 2.67g/cc) in mGal
Gravity_disturbance	Gravity disturbance (residual anomaly after regional removal) in mGal
Grav_FVD	Gravity first vertical derivative (enhances shallow density contrasts)
Grav_THD	Gravity total horizontal derivative (highlights lateral density gradients)

Continuation of table 1

Grav_Gaussian_HP	Gravity high-pass filter (Gaussian filter isolating local high-frequency gravity signal)
Processed_magnetics_RTP	Magnetic intensity, reduced to pole (nT; highlights total field anomalies centered over sources)
Gradient_levelled	Leveled magnetic vertical gradient (nT/m; measured or computed vertical magnetic gradient, leveled)
Mag_FVD	Magnetic first vertical derivative (sharpens shallow magnetic sources)
Mag_THD	Magnetic total horizontal derivative (highlights edges of magnetic bodies)
Mag_Tilt_Derivative	Magnetic tilt derivative (degrees; angle of total field, useful for subtle source detection)
Mag_Analytical_Signal	Magnetic analytic signal amplitude (nT/m; combined 3D gradient magnitude, peaks over magnetic source centers)
Potassium_NASVD	Potassium (% K) from radiometric survey (NASVD noise-filtered)
Uranium_NASVD	Uranium (ppm eU) from radiometric survey (NASVD filtered)
Thorium_NASVD	Thorium (ppm eTh) from radiometric survey (NASVD filtered)
U_Th_ratio	Uranium/Thorium ratio (dimensionless; highlights U enrichment or Th depletion)
U_K_ratio	Uranium/Potassium ratio (dimensionless; can indicate uranium mobility vs K)
Digital_terrain	Digital Terrain Model (m; elevation above sea level)

Methodology

Data Standardization and Feature Selection

All eighteen geophysical and radiometric variables prepared in Section 2.2 were considered during exploratory analysis. For clustering and subsequent quantitative validation, six diagnostic features were retained: Grav_THD, Mag_THD, Mag_Tilt_Derivative, Mag_Analytical_Signal, U/Th, and U/K. This selection was justified by the availability of published threshold intervals and methodological constraints enabling external benchmarking of cluster signatures [10–14]. Variables lacking transferable validation thresholds (e.g., Bouguer anomaly, DTM, and individual K-Th-U channels) were not prioritized for validation due to limited comparability across terrains and potential sensitivity to surficial processes; in particular, K and Th responses may be strongly influenced by regolith and weathering and may not reflect subsurface mineralization [9].

No features were removed or down-weighted within the adopted six-feature workflow. Prior to clustering, each retained feature was standardized to zero mean and unit variance to ensure comparable scaling between gravity derivatives, magnetic derivatives, and radiometric ratios and to prevent dominance of any variable within distance-based clustering.

3.2. Unsupervised clustering algorithms

K-Means clustering was used to obtain hard spatial partitions by minimizing within-cluster variance [10]. Solutions with $k = 3$ and $k = 4$ were evaluated to test partition stability and to assess whether additional clusters produced meaningful spatial structure.

Fuzzy C-Means (FCM) clustering was used to represent gradational boundaries via membership degrees in [0, 1]. The fuzzifier was set to $m = 2$ as a conventional compromise between membership smoothness and numerical stability, and $c = 3$ and $c = 4$ were examined. Membership fields were interpreted as continuous measures of similarity to each cluster.

Self-Organizing Maps (SOM) were trained using a 6×6 lattice to preserve topological relations in the reduced feature space. The MiniSom implementation was used for training and mapping. After convergence, SOM prototypes were aggregated into three groups to obtain a spatial label map consistent with the $k = 3$ partitioning used across methods.

These algorithms were selected to exploit complementary behaviour: compact partitions (K-Means), fuzzy transitions (FCM), and topology-preserving representation (SOM). Supervised

and semi-supervised schemes were not adopted because reliable positive and negative labels were unavailable in this greenfield setting [10].

3.3. Consensus Clustering

To obtain a robust ensemble partition, K-Means, FCM, and SOM were applied independently to the same six standardized features with k (or c) = 3. For FCM, hard labels were derived by selecting the maximum-membership class per sample. For SOM, neuron prototypes were grouped into three clusters and labels were propagated to all samples.

The three label vectors were assembled into an N × 3 label matrix, where each row encoded the triplet of method-specific assignments for one sample. A secondary K-Means run with k = 3 was then performed on this label matrix to derive the final consensus partition (consensus_k3). This strategy was intended to down-weight method-specific artefacts and to emphasize spatial patterns persistent across algorithms [11].

Validation using literature-based feature thresholds

Consensus clusters were validated by comparing their feature-wise mean values to literature-derived anomaly intervals for the six retained features. Threshold ranges reported for potential-field edge detection, tilt derivative and analytic signal applications, as well as radiometric alteration indicators, were used to define expected anomaly magnitudes over structurally complex or mineralization-favourable zones. Because anomaly amplitudes may be attenuated by depth and cover, gravity and magnetic derivative thresholds were adjusted downward by 15–30% to account for amplitude decay. Radiometric thresholds were similarly reduced to account for weathering-related depletion effects reported for uranium and potassium responses in near-surface materials [12].

Threshold Calibration

For cross-feature comparability, both cluster means and threshold bounds were transformed into Z-scores using the global mean (μ) and standard deviation (σ) of each feature:

$$Z = \frac{X - \mu}{\sigma} \tag{1}$$

where μ and σ were computed from the full dataset. A cluster was considered consistent with the benchmark if its standardized mean exceeded the standardized threshold criterion.

To address skewness and to emphasize proportional anomalies, a log10 transformation was additionally applied to selected features (notably ASA and U/K) and to the corresponding thresholds:

$$L = \log_{10}(X) \tag{2}$$

and agreement with benchmark ranges was evaluated in log space. This supplementary check was used to ensure that conclusions were not driven by extreme-value asymmetry and to support interpretation under multiplicative anomaly behaviour [13–15].

Results

Clustering Results

The optimal cluster number was evaluated using the elbow criterion and silhouette scores. A clear inflection and the highest silhouette values were observed at k = 3, whereas improvements beyond k = 3 were marginal and k = 4 produced additional fragmentation, particularly in the eastern sector.

K-Means partitioning with k = 3 produced three spatially coherent domains. The k = 4 solution subdivided the northeastern domain without a clear gain in spatial interpretability. Stable convergence was achieved using multiple random initializations under Lloyd's optimization scheme.

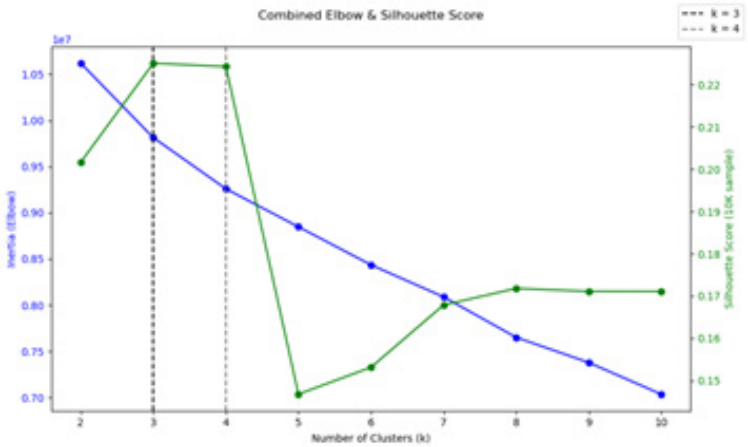

Figure 4 – Elbow method (sum of squared errors versus k)
and silhouette score plot for k = 2-6. The inflection point in the elbow curve
and peak in the silhouette coefficient at k = 3 support the selection of three clusters.

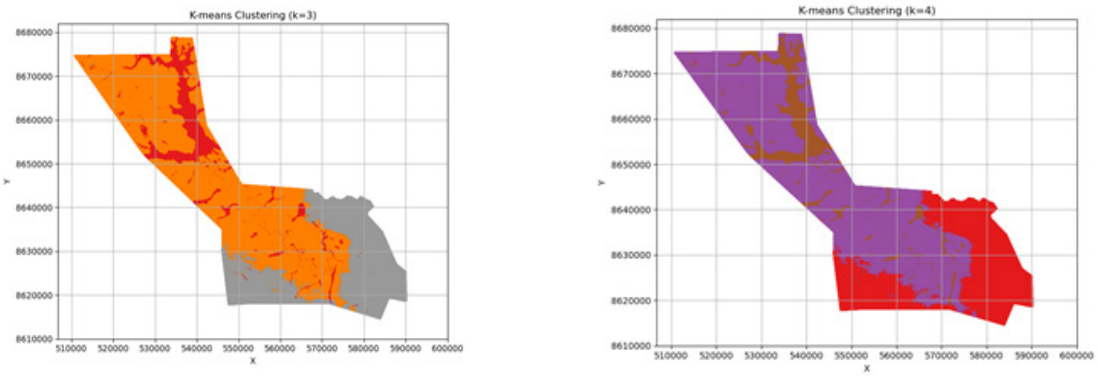

(a) (b)

Figure 5 – K-Means clustering: (a) k = 3 showing three compact zones;
(b) k = 4 illustrating over-fragmentation in the northeast

SOM training on a 6 × 6 lattice yielded 36 prototype neurons summarizing the six-feature input space [16–17]. The resulting neuron map captured local continuity and discontinuity in multivariate geophysical signatures.

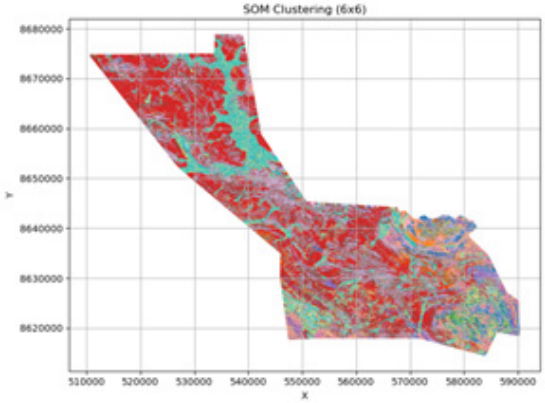

Figure 6 – Self-Organizing Map (6 × 6) projection encoding the six geophysical features onto 36 neurons.
Adjacent neurons on the map correspond to similar input signatures, highlighting local geophysical
variability and structural lineaments

Post-clustering of SOM codebook vectors using K-Means (k = 3) generated smoother, more spatially continuous domains relative to direct K-Means. As with K-Means, the k = 4 variant introduced additional fragmentation.

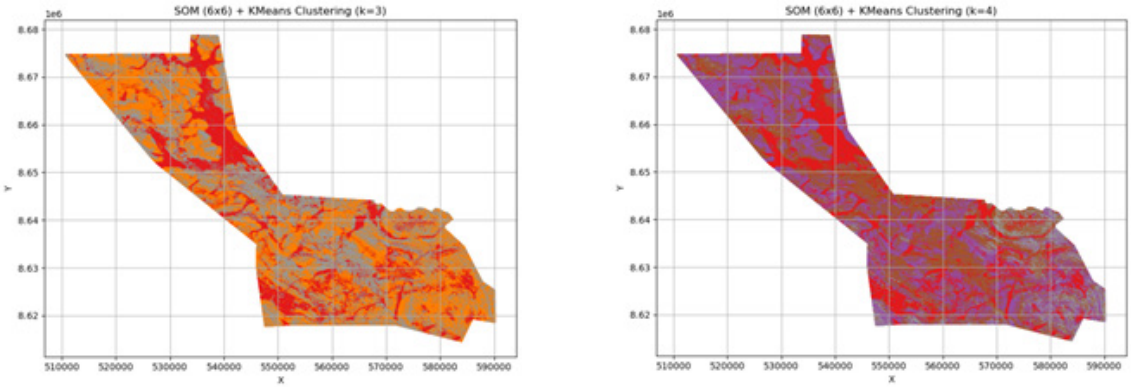

(a) (b)

Figure 7 – Clustering of SOM prototypes with K-Means: (a) k = 3 yields spatially coherent domains; (b) k = 4 introduces unnecessary subdivisions

FCM with m = 2 and c = 3 produced spatial membership gradients, emphasizing transitional zones relative to hard partitioning. The c = 4 variant increased partition complexity with limited additional structure.

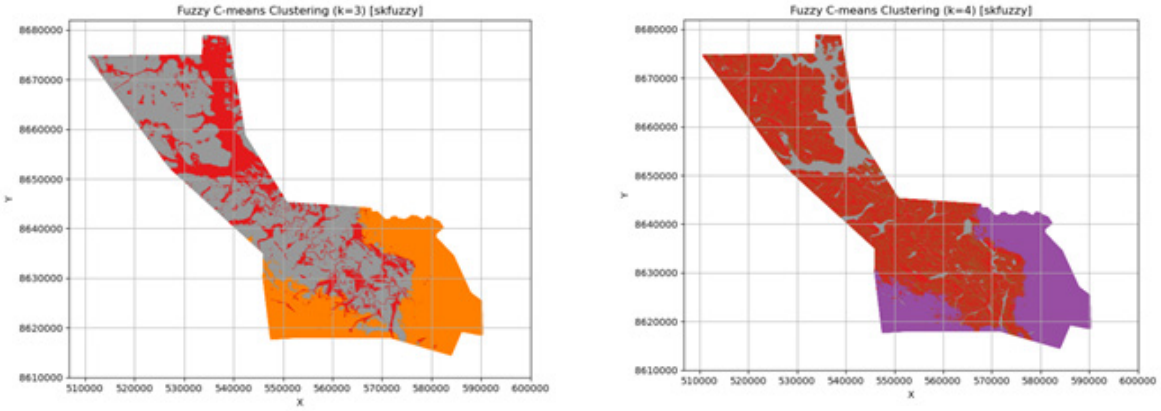

(a) (b)

Figure 8 – Fuzzy C-Means clustering: (a) c = 3 showing membership gradations; (b) c = 4 illustrating increased complexity with limited interpretive gain

Feature discrimination was quantified using ANOVA F-scores computed from cluster partitions. In K-Means, the largest F-scores were associated with gravity and radiometric variables, indicating their dominant role in partition separation. Comparable patterns were observed for FCM and SOM-derived partitions.

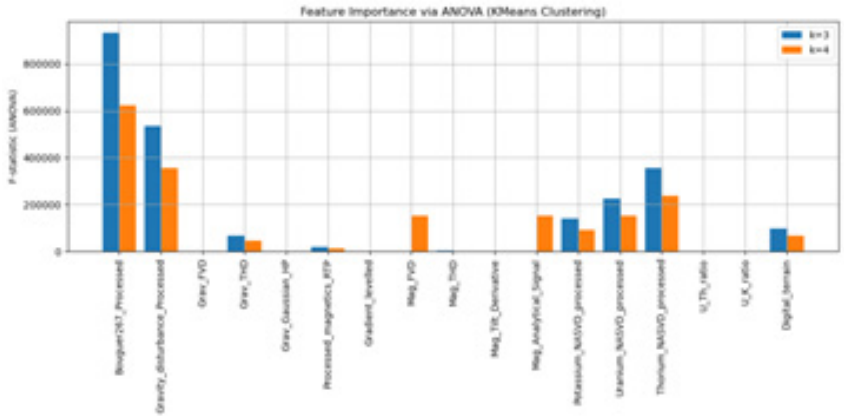

Figure 9 – ANOVA F-values for each geophysical feature in KMeans clustering (k=3 and k=4). Highest discrimination observed for gravity and radiometric features

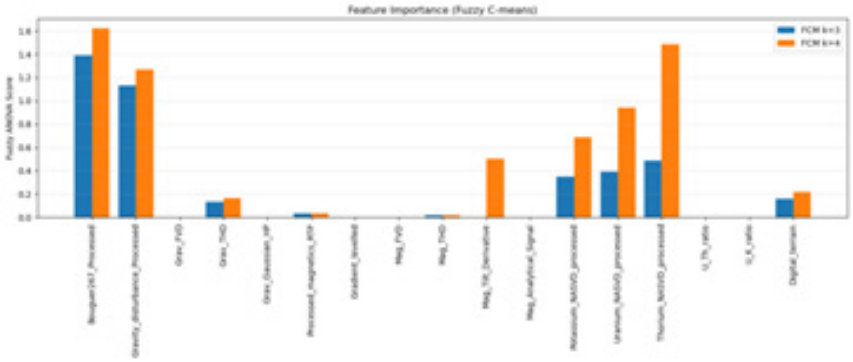

Figure 10 – Feature importance for Fuzzy C-Means clustering based on ANOVA F-scores. The top features align with those found in KMeans

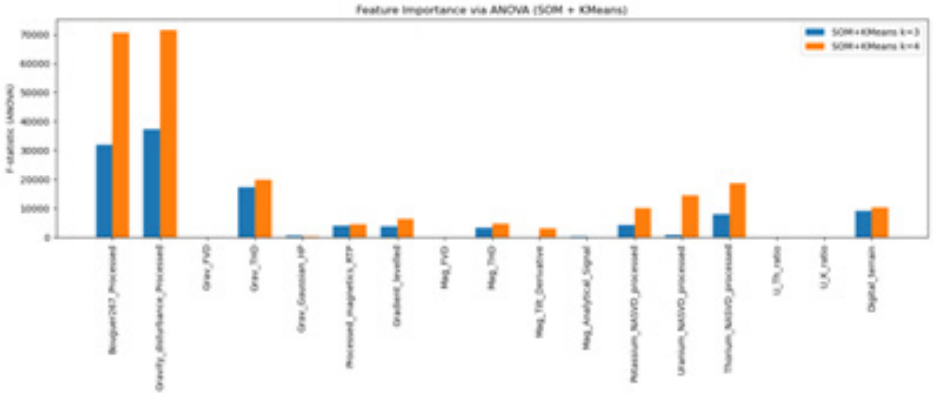

Figure 11 – ANOVA F-values for SOM + KMeans clustering across all features. The results confirm the dominance of gravity and radiometric attributes in cluster differentiation

Consensus clustering was then generated by meta-clustering the label vectors from K-Means, FCM, and SOM using K-Means (k = 3), producing the final consensus_k3 partition. The resulting consensus map highlighted zones of multi-method agreement.

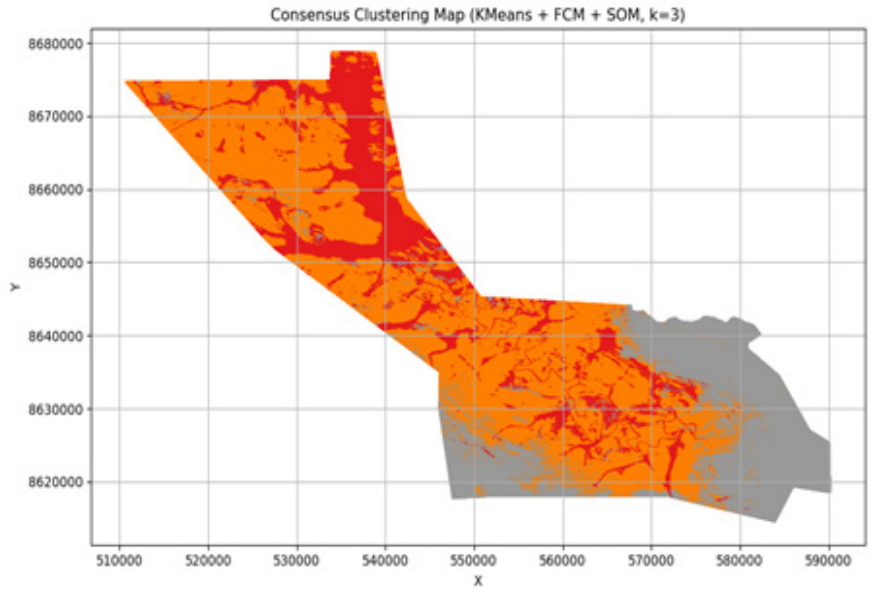

Figure 12 – Consensus clusters (consensus_k3) derived from meta-K-Means on method label vectors. Regions consistently identified by all three methods are emphasized as priority targets

Cluster Validation Against Geophysical Thresholds

Validation of consensus_k3 was performed by comparing feature-wise cluster means with literature-based intervals for six diagnostic variables (Grav_THD, Mag_THD, Mag_Tilt_Derivative, Mag_Analytical_Signal, U/Th, and U/K). The adopted ranges and sources are summarized in Table 2.

Table 2 – Calibrated geophysical intervals used for cluster validation

Feature	Literature Interval	Justification / Source
Grav_THD	0.0025-0.0041	Zhu et al. (2022); Gupta et al. (2018)
Mag_THD	1.66-3.13	Radhakrishna et al. (2014)
Mag_Tilt_Derivative	1.52-1.55	Stewart and Miller (2018)
Mag_Analytical_Signal	150-750	Onyedim and Awoyemi (2005)
U/Th ratio	0.5-1.5	Ciputra et al. (2024)
U/K ratio	5-12	IAEA (2003)

Standardized (Z-score) cluster means were compared against the corresponding standardized threshold bounds, and Cluster 1 was identified as the cluster most consistently meeting or exceeding the benchmark intervals.

A complementary comparison was performed using log10-transformed cluster means and log10-scaled thresholds, confirming the same priority ranking.

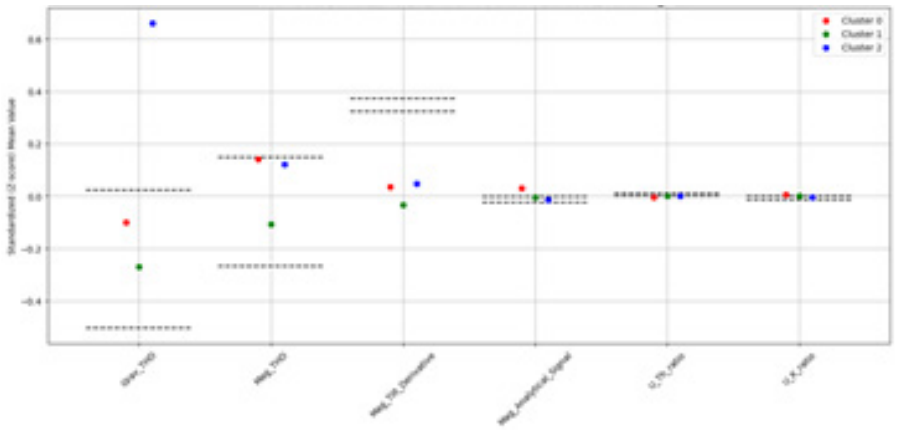

Figure 13 – Standardized (Z-score) cluster means for consensus_k3 compared to literature-based geophysical intervals. Horizontal dashed lines indicate the lower and upper bounds of each threshold interval derived from published studies. Cluster 1 exhibits consistent alignment with or elevation above these bounds across multiple features, reinforcing its geophysical plausibility

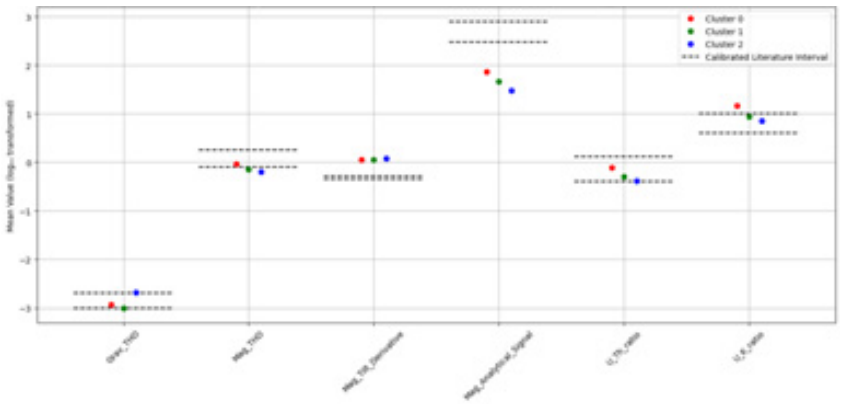

Figure 14 – Log_{10}-transformed cluster means for consensus_k3 compared to log_{10}-scaled intervals. Horizontal dashed lines denote the transformed interval limits

Final Cu-Co Prospectivity Map

A continuous prospectivity map was generated from the FCM membership to the target cluster (Cluster 1, k = 3). Membership values were interpreted as continuous similarity scores to the selected prospective domain.

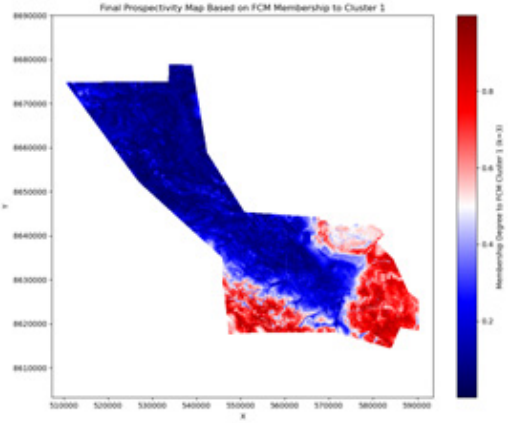

Figure 15 – Continuous prospectivity map based on FCM membership to Cluster 1 (k = 3). Color bar indicates membership values from 0.0 (blue) to 1.0 (red)

For decision-oriented targeting, membership values were discretized into three classes: Low (0.0-0.5), Medium (0.5-0.8), and High (0.8-1.0), based on the empirical membership distribution.

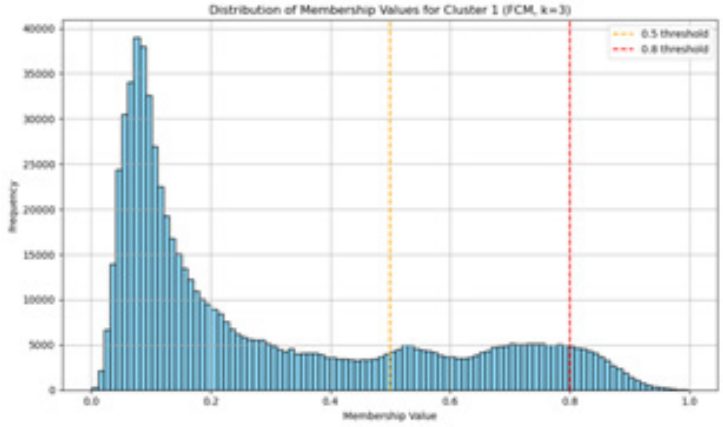

Figure 16 – Distribution of FCM membership values for Cluster 1 (k = 3) with 50 bins. Dashed lines at 0.5 and 0.8 mark the thresholds for medium and high prospectivity classes

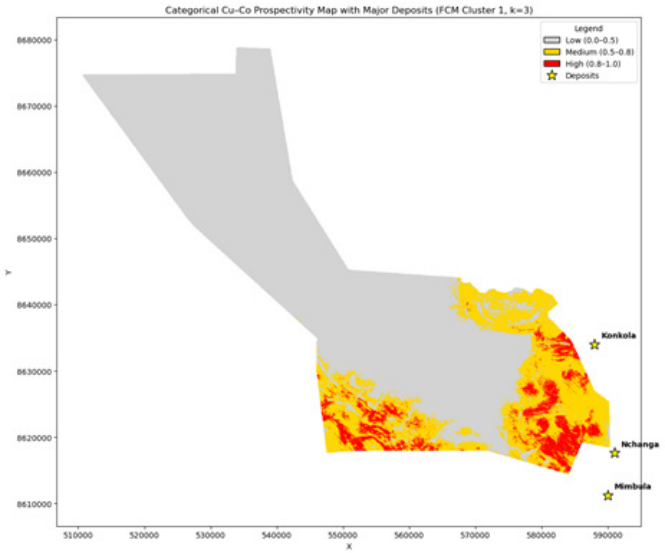

Figure 17 – Categorical Cu-Co prospectivity map (Low/Medium/High) based on FCM membership to Cluster 1 (k = 3)

Thus, the High-prospectivity zones (red) demarcate prime targets for Cu-Co exploration, particularly on the southeastern and southern flanks of the survey area.

Discussion

The results demonstrate that ensemble unsupervised clustering of airborne gravity, magnetic, and radiometric data can delineate structurally coherent Cu-Co target zones in the data-scarce southern Copperbelt margin without the use of labeled training data. By integrating K-Means, Fuzzy C-Means, and Self-Organizing Maps within a consensus framework and validating cluster signatures against literature-derived geophysical intervals, an objective and reproducible targeting scheme was obtained. The high-prospectivity domain forms a spatially coherent belt concentrated in the southern and southeastern sectors of the survey area and occurs in proximity to major stratiform

Cu-Co districts, suggesting consistency with the fold-and-thrust architecture of the Lufilian Arc [18–20]. Elevated magnetic edge indicators and radiometric ratios within the priority cluster are compatible with structurally prepared zones and alteration-related contrasts reported in analogous Cu-Co systems [21–22]. Methodologically, the integration of consensus clustering with quantitative threshold benchmarking reduces subjective cluster selection and mitigates algorithm-specific bias, as recommended in ensemble clustering theory [23], while ensuring consistency with established geophysical anomaly behaviour [24]. Nevertheless, several limitations remain. The absence of drilling or direct geological validation prevents quantitative accuracy assessment; literature-based threshold intervals represent generalized analogues and may not fully capture local lithological or cover variability; radiometric responses may be attenuated by weathering and regolith processes [25]; and multivariate similarity does not guarantee geological uniqueness of causative sources. Therefore, the presented results should be interpreted as a preliminary, data-driven targeting framework requiring subsequent geological verification and potential integration with geochemical or semi-supervised extensions.

Conclusion

A fully unsupervised workflow for delineating prospective stratiform Cu-Co zones in the southern Copperbelt margin (Zambia) has been developed using multi-parameter airborne geophysical data. By combining K-Means, Fuzzy C-Means, and Self-Organizing Maps within a consensus clustering scheme and validating cluster signatures against literature-calibrated geophysical thresholds, a priority cluster was objectively identified and translated into a continuous probabilistic prospectivity map. The selected cluster occupies approximately 12% of the survey area and concentrates exploration focus on the most geophysically anomalous terrain. Spatial concordance with the regional Lufilian structural framework and proximity to established Cu-Co districts support the geological plausibility of the delineated targets [18,19]; however, quantitative validation remains contingent upon ground truth data. The proposed ensemble unsupervised framework provides a reproducible and transferable early-stage targeting approach that can be extended through geochemical integration, weak labeling strategies, and application across other metallogenic provinces.

REFERENCES

1 Ndonfack, K.I.A., Yang, Z., Zhang, J., Whattam, S.A., Xie, Y. Geology, geochemistry, and exploration of the Central African Copperbelt: a review. International Geology Review (2024). http://doi.org/10.1080/00206814.2024.2426200

2 Yousefi, M., Carranza, E.J.M. Data-driven index overlay and Boolean logic mineral prospectivity modeling in greenfields exploration. Natural Resources Research, 25(1), 3–18 (2016). https://doi.org/10.1007/s11053-014-9261-9

3 Saremi, M., Hezarkhani, A., Seyyed Mirzabozorg, S.A.A., DehghanNiri, R., Shirazy, A., Shirazi, A. Unsupervised anomaly detection for mineral prospectivity mapping using Isolation Forest and Extended Isolation Forest algorithms. Minerals, 15(4), 411 (2025). https://doi.org/10.3390/min15040411

4 Xiong, Y., Zuo, R. A positive and unlabeled learning algorithm for mineral prospectivity mapping. Computers & Geosciences, 147, 104667 (2021). https://doi.org/10.1016/j.cageo.2020.104667

5 Wang, C., Chen, J., Ouyang, Y. Determination of predictive variables in mineral prospectivity mapping using supervised and unsupervised methods. Natural Resources Research, 31, 2081–2102 (2022). https://doi.org/10.1007/s11053-021-09930-5

6 Sharapatov, A., Saduov, A., Assirbek, N., Abdyrov, M., Zhumabayev, B. Prediction of rare and anomalous minerals using anomaly detection and machine learning techniques. Applied Computing and Geosciences, 26, 100250 (2025). https://doi.org/10.1016/j.acags.2025.100250

7 Rezapour, M.J., Abedi, M., Bahroudi, A., Rahimi, H. A clustering approach for mineral potential mapping: a deposit-scale porphyry copper exploration targeting. Geopersia, 10(1), 149–163 (2020). http://doi.org/10.22059/geope.2019.284414.648488

8 Martin, R., Boisvert, J. Ensemble spatial and multivariate clustering with geomodeling-specific clustering metrics. Computers & Geosciences, 120, 82–96 (2018). https://doi.org/10.1016/j.cageo.2018.08.005

9 Strehl, A., Ghosh, J. Cluster ensembles – a knowledge reuse framework for combining multiple partitions. Journal of Machine Learning Research, 3, 583–617 (2002). https://doi.org/10.1162/153244303321897735

10 Miller, H.G., Singh, V. Potential field tilt – A new concept for location of potential field sources. Journal of Applied Geophysics, 32(2-3), 213-217 (1994). https://doi.org/10.1016/0926-9851(94)90022-1

11 Cooper, G.R.J. Balancing images of potential-field data. Geophysics, 74(3), L17–L20 (2009). https://doi.org/10.1190/1.3096615

12 Yan, T.-J., Wu, Y.-G., Yuan, Y., Chen, L.-N. Edge detection of potential field data using an enhanced analytic signal tilt angle. Chinese Journal of Geophysics, 59(4), 341-349 (2016).

13 Kianoush, P., Faraj Khah, N.K., Hosseini, S.A., Jamshidi, E., Afzal, P., Ebrahimabadi, A. Geobody estimation by Bhattacharyya method utilizing nonlinear inverse modeling of magnetic data in Baba-Ali iron deposit, NW Iran (2023). https://doi.org/10.21203/rs.3.rs-2433584/v6

14 Abdel-Hakeem, M., El-Tahir, M., Abu Zeid, E., et al. Genetic implications of Th/U, Th/K, and U/K ratios for U mineralizations: a case study from El-Missikat and El-Erediya shear zones, Eastern Desert, Egypt. Geochemical Transactions, 24(1), 3 (2023). https://doi.org/10.1186/s12932-023-00083-3

15 Sharapatov, A., Assirbek, N., Saduov, A., Abdyrov, M., Zhumabayev, B. Consolidated geological and geophysical characteristics of uranium deposit rocks and prospects for their utilization (Shu-Sarysu Province, Kazakhstan). News of the National Academy of Sciences of the Republic of Kazakhstan, Series of Geology and Technical Sciences, 2024(6), 210–229 (2024). https://doi.org/10.32014/2024.2518-170X.471

16 Torremans, K., Gauquier, J., Boyce, A.J., Barrie, C.D., Muchez, Ph., Visser, W., Cnudde, V. Remobilisation features and structural control on ore grade distribution at the Konkola stratiform Cu-Co ore deposit, Zambia. Journal of African Earth Sciences, 79, 10–23 (2013). https://doi.org/10.1016/j.jafrearsci.2012.10.005

17 Cailteux, J.L.H., Kampunzu, A.B., Lerouge, C., Kaputo, A.K., Milesi, J.P. Genesis of sediment-hosted stratiform copper-cobalt deposits, Central African Copperbelt. Journal of African Earth Sciences, 42(1–5), 134–158 (2005). https://doi.org/10.1016/j.jafrearsci.2005.08.001

18 Jackson, M.P.A., Warin, O.N. Neoproterozoic allochthonous salt tectonics during the Lufilian orogeny in the Katangan Copperbelt, central Africa. Geological Society of America Bulletin, 115(3), 314–330 (2003). https://doi.org/10.1130/0016-7606(2003)115<0314:NASTDT>2.0.CO;2

19 Hitzman, M.W., et al. The Central African Copperbelt: diverse stratigraphic, structural, and temporal settings in the world's largest sedimentary copper district. University of Tasmania, Journal contribution (2012). https://hdl.handle.net/102.100.100/572953

20 Sharapatov, A., Saduov, A., Assirbek, N. Sravnitel'nyi analiz vozmozhnostei algoritmov mashinnogo i glubokogo obucheniia v geologii [Comparative analysis of machine and deep learning capabilities in geology]. Nauchno-tekhnicheskii i proizvodstvennyi Gornyi zhurnal Kazakhstana [Scientific-Technical and Industrial Mining Journal of Kazakhstan], 11 (223), 14–21 (2023). https://doi.org/10.48498/minmag.2023.223.11.002 (in Russian).

21 Wilford, J. A weathering intensity index for the Australian continent using airborne gamma-ray spectrometry and digital terrain analysis. Geoderma, 183–184, 124–142 (2012). https://doi.org/10.1016/j.geoderma.2010.12.022

22 Carranza, E.J.M., Hale, M. Where are regional geochemical anomalies found? Geochemistry: Exploration, Environment, Analysis, 1(3), 173–184 (2001). https://doi.org/10.1144/geochem.1.3.173

23 Jain, A.K. Data clustering: 50 years beyond K-means. Pattern Recognition Letters, 31(8), 651–666 (2010). https://doi.org/10.1016/j.patrec.2009.09.011

24 Bezdek, J.C., Ehrlich, R., Full, W. FCM: The fuzzy c-means clustering algorithm. Computers & Geosciences, 10(2–3), 191–203 (1984). https://doi.org/10.1016/0098-3004(84)90020-7

25 Sharapatov, A., Zhumabayev, B.T., Saduov, A.B., Assirbek, N. Geomagnitnye dannye i ikh ispol'zovanie pri reshenii zadach geonauk [Geomagnetic data and their use in solving geoscience problems]. Nauchno-tekhnicheskii i proizvodstvennyi Gornyi zhurnal Kazakhstana [Scientific-Technical and Industrial Mining Journal of Kazakhstan], 12 (224), 30–36 (2023). https://doi.org/10.48498/minmag.2023.224.12.004 (in Russian).

[1]*Садуов А.,
аға оқытушы, ORCID ID: 0000-0003-1501-7772
e-mail: a.saduov@satbayev.university

[1]Satbayev University, Алматы қ., Қазақстан

ЗАМБИЯДАҒЫ МЫС БЕЛДЕУІНІҢ ОҢТҮСТІК ЖИЕГІНДЕ СТРАТИФОРМДЫ МЫС-КОБАЛЬТ МИНЕРАЛДАНУЫНЫҢ ПЕРСПЕКТИВАЛЫҚ АЙМАҚТАРЫН МҰҒАЛІМСІЗ ОҚЫТУ ӘДІСТЕРІ НЕГІЗІНДЕ АЙҚЫНДАУ

Аңдатпа

Мақалада Орталық Африка Мыс белдеуінің оңтүстік жиегінде (Замбия) орналасқан стратиформды мыс-кобальт минералдануының перспективалы аймақтарын тек аэрогеофизикалық деректер негізінде айқындауға арналған тәсіл ұсынылған. Пайдаланылған деректер гравиметриялық, магниттік, радиометриялық және бедерлік параметрлерді қамтиды. Талдау барысында кластерлеудің үш алгоритмі – K-Means, Fuzzy C-Means (FCM) және Кохоненнің өзін-өзі ұйымдастыратын карталары (Self-Organizing Maps, SOM) қолданылып, кейін олардың нәтижелері тұрақты мақсатты аймақтарды бөліп көрсету мақсатында консенсустық кластерлеу аясында біріктірілді. Әрбір кластер үшін негізгі геофизикалық туынды көрсеткіштер, оның ішінде еңіс туындысы, толық көлденең туынды және аналитикалық сигнал, сондай-ақ U/Th және U/K радиометриялық қатынастары есептеліп, өзара салыстырылды. Ең перспективалы кластер әдебиеттерге негізделген геофизикалық шекті мәндер арқылы валидацияланып, оның белгілі іздеу критерийлері мен өңірлік құрылымдық заңдылықтарға сәйкес келетіні көрсетілді. Қорытынды перспективалылықтың ықтималдық картасы FCM алгоритмінің мүшелік мәндері негізінде құрастырылып, кейін сенімділіктің үш деңгейіне жіктелді. Бұрғылау деректерінің болмауы нәтижелердің дәлдігін тікелей сандық бағалауға мүмкіндік бермегенімен, алынған қорытындылар көппараметрлі аэрогеофизикалық деректерге қолданылған мұғалімсіз оқыту әдістерінің геологиялық ақпарат тапшы жағдайларда барлау жұмыстарының бастапқы кезеңдерінде тиімді пайдаланылуы мүмкін екенін көрсетті. Ұсынылған тәсілді аз зерттелген аумақтарда жасанды интеллектке негізделген перспективалылықты бағалаудың қайта жаңғыртылатын әдістемелік негізі ретінде қарастыруға болады.

Түйін сөздер: мыс-кобальт, мұғалімсіз оқыту, кластерлеу, аэрогеофизика, перспективалықты болжау, Замбия.

[1]*Садуов А.,
ст. преподаватель, ORCID ID: 0000-0003-1501-7772,
e-mail: a.saduov@satbayev.university

1Satbayev University, г. Алматы, Казахстан

ВЫДЕЛЕНИЕ ЗОН ПЕРСПЕКТИВНОСТИ СТРАТИФОРМНОЙ МЕДНО-КОБАЛЬТОВОЙ МИНЕРАЛИЗАЦИИ НА ОСНОВЕ МЕТОДОВ ОБУЧЕНИЯ БЕЗ УЧИТЕЛЯ НА ЮЖНОЙ ОКРАИНЕ МЕДНОГО ПОЯСА (ЗАМБИЯ)

Аннотация

В статье представлен подход к выделению перспективных зон стратиформной медно-кобальтовой минерализации на южной окраине Центрально-Африканского Медного пояса (Замбия) на основе исключительно аэрогеофизических данных, включающих гравиметрические, магнитные, радиометрические и топографические параметры. Для анализа были использованы три алгоритма кластеризации – K-Means, Fuzzy C-Means (FCM) и самоорганизующиеся карты Кохонена (Self-Organizing Maps, SOM), после чего результаты были объединены в рамках консенсусной кластеризации для выделения устойчивых целевых зон. По каждому кластеру были рассчитаны и сопоставлены ключевые геофизические производные, включая производную наклона, полную горизонтальную производную и аналитический сигнал, а также радиометрические

отношения U/Th и U/K. Наиболее перспективный кластер был валидирован по литературно обоснованным геофизическим пороговым значениям и показал соответствие известным поисковым критериям и региональным структурным закономерностям. Итоговая вероятностная карта перспективности была построена по значениям принадлежности FCM и дополнительно разделена на три уровня уверенности. Несмотря на отсутствие буровых данных, не позволяющее выполнить прямую количественную оценку точности, полученные результаты показывают, что методы обучения без учителя, примененные к многопараметрическим аэрогеофизическим данным, могут эффективно использоваться для ранних стадий поисково-разведочных работ в условиях дефицита геологической информации. Предложенный подход может рассматриваться как воспроизводимая основа для ИИ-ориентированного прогнозирования перспективности в слабо изученных территориях.

Ключевые слова: медь-кобальт, обучение без учителя, кластеризация, аэрогеофизика, прогнозирование перспективности, Замбия.